Competition between antiferromagnetism and superconductivity in a doped Hubbard model with anisotropic interaction

Runyu Ma [1,2] and Tianxing Ma [1,3,*]

[1]*Department of Physics, Beijing Normal University, Beijing 100875, China*
[2]*Beijing Computational Science Research Center, Beijing 100193, China*
[3]*Key Laboratory of Multiscale Spin Physics (Ministry of Education), Beijing Normal University, Beijing 100875, China*

The competition between antiferromagnetism and superconductivity is one of the central questions in research involving strongly correlated systems. In this paper, we utilize a double-layer model containing Hubbard interaction and interlayer Heisenberg interaction to reveal their competition. This model is free of the sign problem under certain conditions, and we perform projector quantum Monte Carlo simulations to extract the ground-state correlations of magnetism and superconductivity. Our results show that the superconductivity emerges when the antiferromagnetism is suppressed by tuning the filling or the anisotropy of the interlayer Heisenberg interaction. This model can be seen as an analog of unconventional superconductors and may help us to understand the transition from an antiferromagnetic insulator to a superconductor.

I. INTRODUCTION

It is widely known that unconventional superconductors may have magnetic parents [1]. Since the discovery of superconductivity in doped cuprates [2], a large number of experiments have been conducted to explore its mechanism and complex phase diagram [3–5], especially the transition from an antiferromagnetic (AFM) insulator to a superconductor, which is a critical part of the study of unconventional superconductivity. Constructing a theoretical model that can describe these phenomena, especially the competition between antiferromagnetism and superconductivity, is an important problem for condensed matter physicists. Hubbard-like models have proven to be good candidates to describe AFM insulators [6–8] and superconductors [3,9–11]. However, because of the exponential growth of Hilbert space, the introduction of strong electronic interaction brings new challenges to solving this model.

Many numerical methods have been developed to solve the Hubbard model and its extensions, for example, the density matrix renormalization group method [12], the quantum Monte Carlo method [13], dynamic mean field theory [14], and so on. Among them, the quantum Monte Carlo method is a great method owing to its advantage of accuracy and the convenience of use in some sense, and it has been used to extract ground-state or finite-temperature properties of strongly correlated systems. In past decades, quantum Monte Carlo simulations of Hubbard-like models have achieved fruitful results, including pairing symmetries [15–18], a charge density wave state [19], localization of electronic states [20–22], unconventional superconductivity in twisted bilayer graphene [23–26], and stripe order in two-dimensional electronic correlated systems [27,28].

As an analog to the cuprate superconductors, we are particularly interested in the doping case where superconductivity emerges. However, quantum Monte Carlo algorithms are limited by the sign problem, especially when we want to use them to investigate the transition from an AFM insulator to a superconductor. At finite doping where superconductivity emerges, the sign problem is severe in the original Hubbard model and undermines the accuracy of simulations. There are some works that attempt to eliminate or alleviate the sign problem, for example, by expressing spinless fermions in a Majorana representation, which can make the simulations avoid the sign problem [29], by adiabatically switching on the electronic interaction [30], or by constraining the phase space [31]. There are also some works that attempt to utilize the sign problem to analyze quantum critical points [32]. In addition, the sign problem can be eliminated by some special symmetries. For example, a bipartite lattice such as a square or honeycomb lattice can avoid the sign problem at half filling because of the particle-hole symmetry. Another example is the attractive Hubbard model; it can avoid the sign problem at arbitrary filling, because after Hubbard-Stratonovich (HS) transformation in the charge channel, spin up is identical to spin down, and so its determinant is positive definite.

Recently, a sign-free extended bilayer Hubbard-like model—a generalized Scalapino-Zhang-Hanke model—has been utilized to investigate the transition from the AFM insulating state to the superconducting (SC) state [33], which provides an excellent platform to study unconventional superconductivity. Through time-reversal symmetry, this effective model is free of the sign problem at arbitrary filling. It was shown that a quantum phase transition occurs from an Ising anisotropic AFM insulating phase or an SU(2) invariant Mott insulating phase without the AFM ordering to a rung-singlet SC phase with an extended *s*-wave symmetry driven by doping. This is an attractive feature to conduct quantum Monte

---

*txma@bnu.edu.cn

Carlo simulations at finite doping. However, in that work, the parameters were confined to a relatively small region at some fixed terms, to establish AFM long-range order at half filling.

The interlayer or interorbital interactions may play an important role in some certain materials, such as monolayer FeSe [34]. These kinds of interactions can be implemented in ultracold-atom experiments [35]. So, in this paper we conduct a more comprehensive investigation of this extended bilayer Hubbard model and its interlayer interactions by using the projector quantum Monte Carlo (PQMC) algorithm to extract the ground-state properties of this system. We have tuned the strength and the anisotropy of the interlayer Heisenberg interaction, and we find some interesting behaviors which were not revealed in the previous work. By calculating the correlation lengths and using the finite-size scaling technique, we carefully investigate the magnetism and superconductivity in this model. We find that the system is sensitive to both the doping and the anisotropy of interlayer interaction. The antiferromagnetism will fade away when hole doping is introduced, and then superconductivity appears. At the same doping, the anisotropy of interlayer interaction also affects the superconductivity and magnetism, where the $J_\perp$ part of the Heisenberg interaction may be a critical component when SC pairs are taking shape. In some sense, this interlayer Heisenberg interaction is similar to the t-J model, which can be considered as a good starting point to study cuprate superconductors [36]. The t-J model contains Heisenberg interactions at the nearest neighbor. This is different from our model, which possesses only interlayer interactions, and then we have different pairing symmetries. However, the mechanics behind them may be the same. Our results reveal the competition between antiferromagnetism and superconductivity in a numerically exact manner, which is important for us to understand the transition from an AFM insulator to a superconductor.

II. MODEL AND METHOD

The effective model we construct is on a two-layer square lattice, including a Hubbard interaction term and an anisotropic Heisenberg interaction term [37,38]. The Hamiltonian can be written as follows:

$$
\begin{aligned}
H = &-t \sum_{\langle \mathbf{i},\mathbf{j}\rangle, l\sigma} c_{\mathbf{i}l\sigma}^\dagger c_{\mathbf{j}l\sigma} \\
&+ \sum_{\mathbf{i}} [g_1 (c_{\mathbf{i}1\uparrow}^\dagger c_{\mathbf{i}1\uparrow} - c_{\mathbf{i}1\downarrow}^\dagger c_{\mathbf{i}1\downarrow} - c_{\mathbf{i}2\uparrow}^\dagger c_{\mathbf{i}2\uparrow} + c_{\mathbf{i}2\downarrow}^\dagger c_{\mathbf{i}2\downarrow})^2 \\
&+ g_2 (c_{\mathbf{i}1\uparrow}^\dagger c_{\mathbf{i}1\downarrow} + c_{\mathbf{i}1\downarrow}^\dagger c_{\mathbf{i}1\uparrow} - c_{\mathbf{i}2\uparrow}^\dagger c_{\mathbf{i}2\downarrow} - c_{\mathbf{i}2\downarrow}^\dagger c_{\mathbf{i}2\uparrow})^2 \\
&+ g_2 (-ic_{\mathbf{i}1\uparrow}^\dagger c_{\mathbf{i}1\downarrow} + ic_{\mathbf{i}1\downarrow}^\dagger c_{\mathbf{i}1\uparrow} + ic_{\mathbf{i}2\uparrow}^\dagger c_{\mathbf{i}2\downarrow} - ic_{\mathbf{i}2\downarrow}^\dagger c_{\mathbf{i}2\uparrow})^2] \\
= &-t \sum_{\langle \mathbf{i},\mathbf{j}\rangle, l\sigma} c_{\mathbf{i}l\sigma}^\dagger c_{\mathbf{j}l\sigma} + \sum_{\mathbf{i}} \left[J_z S_{\mathbf{i}1}^z S_{\mathbf{i}2}^z + \frac{1}{2} J_\perp (S_{\mathbf{i}1}^+ S_{\mathbf{i}2}^- + S_{\mathbf{i}1}^- S_{\mathbf{i}2}^+) \right] \\
&+ \sum_{\mathbf{i}} U (n_{\mathbf{i}1\uparrow} n_{\mathbf{i}1\downarrow} + n_{\mathbf{i}2\uparrow} n_{\mathbf{i}2\downarrow}) - \frac{U}{2} N,
\end{aligned}
\tag{1}
$$

where we define $U = -2g_1 - 4g_2$, $J_z = -8g_1$, and $J_\perp = -8g_2$ for notational convenience. In this equation, $c_{\mathbf{i}l\sigma}$ ($c_{\mathbf{i}l\sigma}^\dagger$) means annihilating (creating) an electron at site $\mathbf{i}$, layer $l = 1, 2$, spin $\sigma = \uparrow, \downarrow$, and $\langle \mathbf{i},\mathbf{j}\rangle$ indicates the nearest neighbor. In

addition, $S_{\mathbf{i}l}^z = \frac{1}{2} n_{\mathbf{i}l\uparrow} - \frac{1}{2} n_{\mathbf{i}l\downarrow}$, $S_{\mathbf{i}l}^{+/-} = c_{\mathbf{i}l\uparrow/\downarrow}^\dagger c_{\mathbf{i}l\downarrow/\uparrow}$, and $n_{\mathbf{i}l\sigma} = c_{\mathbf{i}l\sigma}^\dagger c_{\mathbf{i}l\sigma}$. We set $t = 1$ as a unit of energy in this paper.

The main idea of the PQMC algorithm is to apply a projector to a trial wave function $|\Psi_T\rangle$, and the observables can be computed as

$$
\langle \hat{O} \rangle = \lim_{\beta \to \infty} \frac{\langle \Psi_T | e^{-\beta \hat{H}/2} \hat{O} e^{-\beta \hat{H}/2} |\Psi_T\rangle}{\langle \Psi_T | e^{-\beta \hat{H}} |\Psi_T\rangle}.
\tag{2}
$$

The discrete HS transformation is performed; we use the four-component HS transformation, namely, $e^{\Delta\tau\lambda A^2} \approx \frac{1}{4} \sum_{l=\pm 1, \pm 2} \gamma(l) e^{\sqrt{\Delta\tau\lambda}\eta(l)A}$, where A is an operator and $\gamma(\pm 1) = 1 + \sqrt{6}/3$, $\gamma(\pm 2) = 1 - \sqrt{6}/3$ and $\eta(\pm 1) = \pm\sqrt{2(3 - \sqrt{6})}$, $\eta(\pm 2) = \pm\sqrt{2(3 + \sqrt{6})}$.

$$
\frac{\langle \Psi_T | e^{-\beta \hat{H}/2} \hat{O} e^{-\beta \hat{H}/2} |\Psi_T\rangle}{\langle \Psi_T | e^{-\beta \hat{H}} |\Psi_T\rangle} \approx \sum_s \mathbf{P}_s \langle \hat{O} \rangle_s,
\tag{3}
$$

where $\langle \hat{O} \rangle_s = \frac{\langle \Psi_T | e^{-\beta \hat{H}_s/2} \hat{O} e^{-\beta \hat{H}_s/2} |\Psi_T\rangle}{\langle \Psi_T | e^{-\beta \hat{H}_s} |\Psi_T\rangle}$ is the expectation at a certain auxiliary field s; here, H_s is the decomposed Hamiltonian, namely, $e^{-\beta H_s} = \prod_\tau e^{-\Delta\tau H_0} \prod_i \gamma(s_{\tau,i}) e^{\sqrt{-\Delta\tau g}\eta_{\tau,i} H_{I,i}}$ (H_0 is the free part of the original Hamiltonian, and $H_{I,i}$ is the interaction operator at site i). $\mathbf{P}_s = \frac{\det(P^\dagger e^{-\beta \hat{H}_s} P)}{\sum_s \det(P^\dagger e^{-\beta \hat{H}_s} P)}$ (P is the matrix form of $|\Psi_T\rangle$) can be seen as the weight of Monte Carlo sampling. In general, $\mathbf{P}_s$ is not positive definite; then the sign problem occurs.

In this paper, we resort to time-reversal symmetry to avoid the sign problem, which restricts the form of interaction. If the action after HS transformation possesses time-reversal symmetry [37], its eigenvalues are always complex-conjugate pairs; this ensures the positive definiteness of its determinant. As for Eq. (1), if g_1 and g_2 are both negative, the matrix after HS transformation $\hat{H}_s$ has time-reversal symmetry, and this can ensure the positive definiteness of $\mathbf{P}_s$. For more details, see Refs. [37,38]. Our QMC simulations employ the projector scheme working at zero temperature with the projection time $\beta = 4L$ and the discrete imaginary time slice $\Delta\tau = 0.1$. We use a noninteracting ground-state wave function as the trial wave function, and random chemical potentials are added on every site; otherwise the degeneracy would break the wave function's symmetries and lead to the sign problem. The random potentials added can be written down as $H_{rp} = -\sum_i d_i (n_{\mathbf{i}1\uparrow} + n_{\mathbf{i}1\downarrow} + n_{\mathbf{i}2\uparrow} + n_{\mathbf{i}2\downarrow})$, where d_i is a uniform random number in $[0, 0.01)$ generated at site i.

Next, we define antiferromagnetic and superconducting orders and their correlations,

$$
S(\mathbf{k}) = \frac{1}{L^2} \sum_{\mathbf{i},\mathbf{j}} e^{-i\mathbf{k}\cdot(\mathbf{R_i}-\mathbf{R_j})} \cdot \langle (S_{\mathbf{i}1}^z - S_{\mathbf{i}2}^z)(S_{\mathbf{j}1}^z - S_{\mathbf{j}2}^z) \rangle,
\tag{4}
$$

where L is lattice size, and we denote $S_{\text{AFM}} = S(\pi, \pi)$. The SC correlation is defined as

$$
P(\mathbf{k}) = \frac{1}{L^2} \sum_{\mathbf{i},\mathbf{j}} e^{-i\mathbf{k}\cdot(\mathbf{R_i}-\mathbf{R_j})} \cdot \langle \Delta_{\mathbf{i}}^\dagger \Delta_{\mathbf{j}} \rangle,
\tag{5}
$$

where $\Delta_{\mathbf{i}} = c_{\mathbf{i}1\uparrow} c_{\mathbf{i}2\downarrow} - c_{\mathbf{i}1\downarrow} c_{\mathbf{i}2\uparrow} + c_{\mathbf{i}2\uparrow} c_{\mathbf{i}1\downarrow} - c_{\mathbf{i}2\downarrow} c_{\mathbf{i}1\uparrow}$, and we denote $P_{\text{SC}} = P(0, 0)$.

One of the major challenges is the great computational cost, and most of our results are confined to system size $L = 8$.
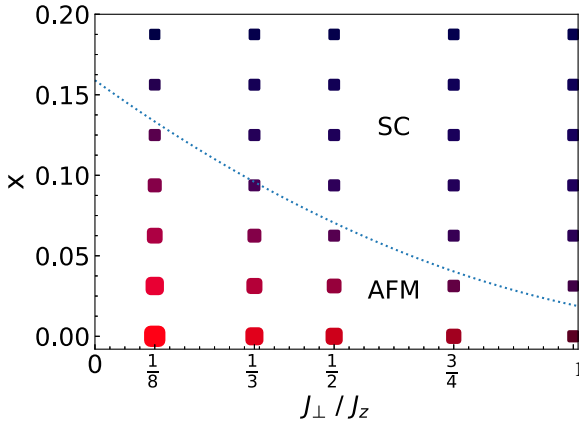
FIG. 1. An illustration of phase at $L = 8$ and $U = 1.25$. The size of the symbols indicates the value of the correlation lengths among SC and AFM states. The color of the symbols indicates the difference between them. The larger the AFM (SC) correlation length is, the more red (blue) the symbol is. The dotted line indicates the approximate boundary between them. The x axis is the value of $J_\perp/J_z$, and the y axis is the doping.

To characterize the competition quantitatively at a fixed system size, we resort to the correlation length, defined as [39,40]

$$\xi(L)^2 = \frac{1}{4\sin(\pi/L)^2}\left(\frac{C_k}{C_{k+\delta k}} - 1\right), \qquad (6)$$

where δk is the minimum momentum of size L and C_k can be one of P_{SC} or S_{AFM}. The correlation length may not reflect the long-range order accurately since our simulations are confined to a small lattice size, but it can reveal the competition between observables directly.

III. RESULTS AND DISCUSSION

To illustrate the competition between antiferromagnetism and superconductivity, we compare the correlation lengths of SC and AFM states at different hole dopings and $J_\perp/J_z$. $J_\perp/J_z$ reflects the anisotropy of interlayer interaction, and $J_\perp = J_z$ represents that there is an isotropic Heisenberg interaction between two layers. We start by investigating the correlation lengths at different $J_\perp$ and J_z while fixing the value of $U = -\frac{J_z}{4} - \frac{J_\perp}{2}$, and the results are shown in Fig. 1.

Figure 1 directly reveals the competition between antiferromagnetism and superconductivity. The advantage of this model is that one can enhance AFM or SC order by tuning the parameters in Hamiltonian equation (1). The system favors SC order when $J_\perp$ is larger and favors AFM order when J_z is larger. A more evident display of this phenomenon is shown in Fig. 2, where we can see that increasing the value of $J_\perp/J_z$ may inhibit the AFM order and enhance the SC order.

Then, we increase J_z and $J_\perp$ simultaneously, while keeping $J_\perp/J_z = 1$, for which the correlation length is shown in Fig. 3. We can see that the AFM correlation length does not increase monotonically as U increases. It starts to decline when $U \approx 1.25$, accompanied by the decreasing of SC correlation lengths. At half filling, although the magnetic order has been suppressed by changing $J_\perp/J_z$, superconductivity is always
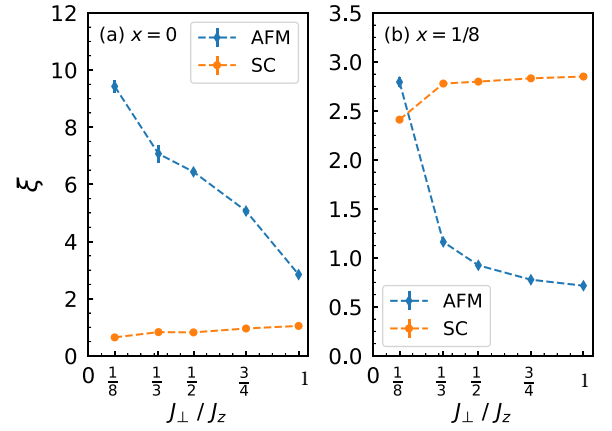
absent. This might imply that there is another order we have not discussed and the relationship between SC and AFM is more complex at larger U values.

The disappearance of AFM can also be confirmed by finite-size scaling. Based on the scaling hypothesis $S_{AFM}(L)/L^2 = a + b/L + c\xi^2/L^2$, we extrapolate $S_{AFM}(L)/L^2$ to the thermodynamic limit [41]. Besides, the b term can be ignored in the AFM extrapolation since it comes from gapless excitations. These results are shown in Fig. 4, where long-range AFM order develops at small U and starts to be inhibited as U gets larger.

The disappearance of AFM has not been observed in a single-layer Hubbard model. Recall the definition of U, J_z, and $J_\perp$: $U = -2g_1 - 4g_2$, $J_z = -8g_1$, and $J_\perp = -8g_2$. The interlayer Heisenberg interaction is proportional to the Hubbard interaction: $4U = J_z + 2J_\perp$. When the interlayer interaction become stronger, the intralayer AFM order becomes more and more negligible. As shown in Fig. 5, antiparallel

FIG. 2. Correlation lengths at $L = 8$ and $U = 1.25$ at (a) half filling and (b) $x = \frac{1}{8}$ doping with different J_z and $J_\perp$. As $J_\perp/J_z$ increases, the SC correlation length increases and the AFM correlation length decreases; the AFM state is more sensitive to $J_\perp/J_z$ than the SC state is.
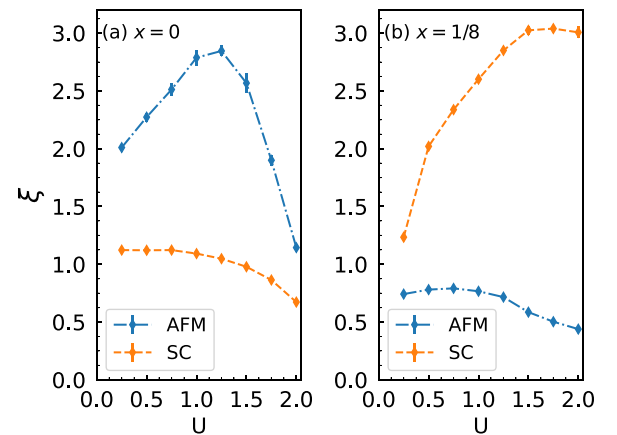

FIG. 3. Correlation lengths at $L = 8$ and $J_z = J_\perp$. (a) At half filling, the AFM strength increases at first and then decreases quickly, and the peak is around $U = 1.25$. The SC strength also drops around $U = 1.0$. (b) At $x = \frac{1}{8}$ for doping, the AFM strength decreases monotonically, and the SC strength increases monotonically.
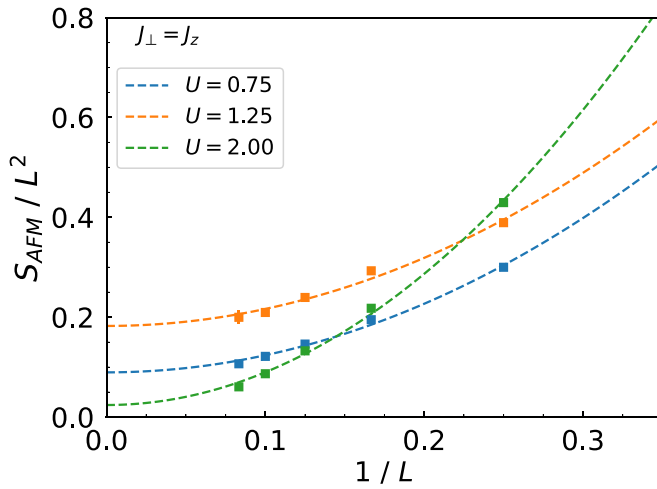
FIG. 4. Finite-size scaling of S_{AFM} at half filling for $J_z = J_\perp$. One can see that the residual at the thermodynamic limit at $U = 2.00$ is much smaller than that at $U = 1.25$. This is consistent with correlation lengths shown in Fig. 2.

spins allow a virtual hopping process, and this process will cause the energy of the system to become higher, since the interlayer interaction will no longer contribute a negative value of energy if the electron is hopping to another site. In contrast, parallel spins forbid this virtual hopping process and may have lower energy.

In Fig. 3, we can also see that correlations of SC and AFM are changed by the doping. At $\frac{1}{8}$ doping, shown in Fig. 3(b), the SC correlation length increases monotonically as U increases, while AFM correlation length decreases. This indicates that the increasing interaction strength always suppresses AFM order and favors SC order at finite doping. Next, we show the doping dependence of AFM and SC orders. From Fig. 6, one can see that the SC order prefers finite doping, and the optimal doping is dependent on $J_\perp / J_z$. At $J_z = J_\perp$, the optimal doping is around $\frac{1}{10}$. It gets larger as J_z increases, and at $J_\perp / J_z = \frac{1}{8}$ it is around $\frac{1}{6}$.

Because the maximum of SC correlation lengths is smaller than that of AFM correlation lengths, we extrapolate the SC structure factor to the thermodynamic limit in Fig. 7 to confirm the long-range properties of SC. At $L = 10$ and $L = 6$, $\frac{1}{8}$ doping corresponds to hole numbers of 25 and 9, respectively; these are not closed-shell fillings, and we average the SC correlations of the nearest closed-shell fillings around them.
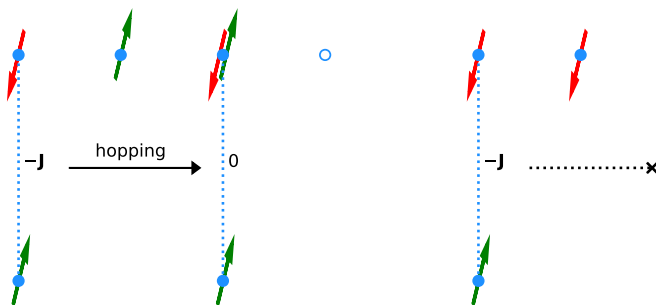

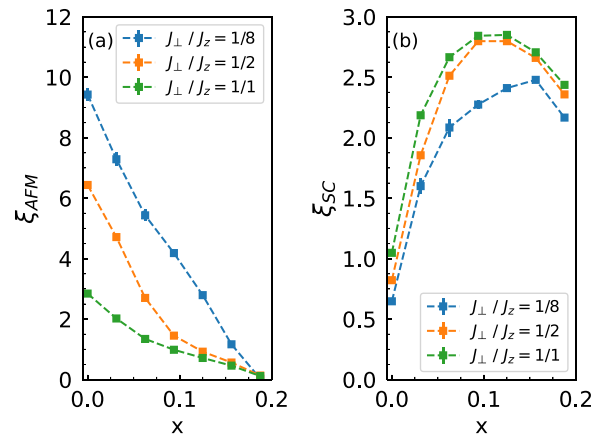FIG. 5. A sketch of spin configuration shows that the interlayer interaction affects the intralayer order.

FIG. 6. AFM and SC correlation length at different electron numbers and with U fixed at 1.25. (a) AFM orders prefer large J_z and half filling, while (b) SC orders prefer large $J_\perp$ and finite doping.

From the finite-size scaling results, one can see that SC long-range order would be established with the proper choice of parameters. These results indicate that larger U and $J_\perp$ favor SC order at finite doping.

Finally, we check the effects of system size. Most of our results are simulated on a lattice with $L = 8$, and in that case there are 2×8^2 sites in total, which is fairly large. We choose this relatively large lattice size because of the special form of interaction in Hamiltonian equation (1). In our PQMC simulations, the computational cost is nearly the same as that for simulations on 4×8^2 sites of an ordinary Hubbard model. In Fig. 8, we show the SC and AFM correlation lengths at different lattice sizes. One can see that, in some sense, $L = 8$ is not large enough; when finite-size scaling results assert that there is AFM or SC long-range order, the corresponding ξ / L is still increasing. So we cannot use ξ at $L = 8$ to assert whether there is a long-range order or not. Fortunately, the results at different L are qualitatively consistent with each other, and so the correlation lengths ξ can be used to compare the strengths of SC and AFM. For analysis of long-range order, we still resort to finite-size scaling.
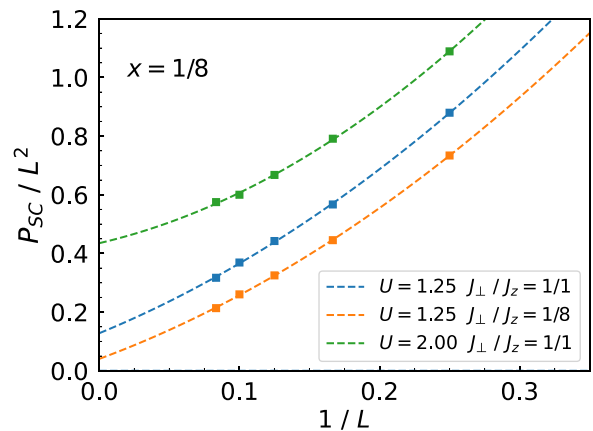

FIG. 7. Extrapolations of SC correlations at $L = 8$ and $x = \frac{1}{8}$. The SC strength becomes larger when either U increases or $J_\perp$ increases. This is consistent with correlation lengths we computed before.
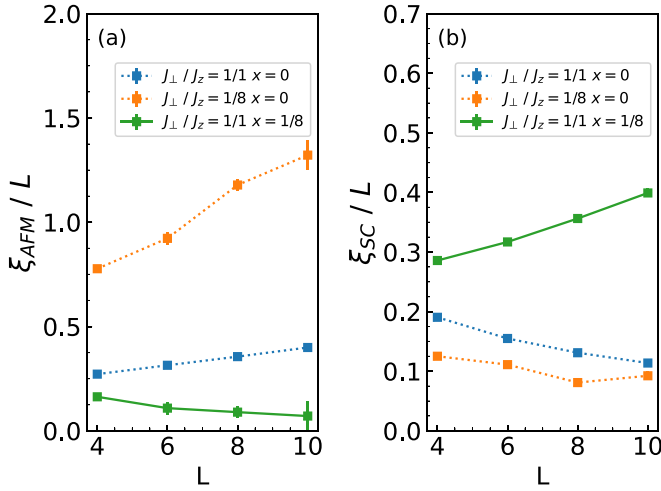
FIG. 8. Correlation lengths at different lattice sizes: (a) AFM and (b) SC. In this figure, dotted lines are at half filling, and solid lines are at $\frac{1}{8}$ doping; $U = 1.25$ is fixed. We can see that the results at $L = 8$ can characterize the properties of the system qualitatively, and so we may use those results to reveal the competition between antiferromagnetism and superconductivity.

IV. SUMMARY

In this paper, we utilize a sign-problem-free model to investigate the competition between SC and AFM order. By performing PQMC simulations, we compare the correlation lengths at different parameter values and use the finite-size scaling technique to study the long-range behaviors. Our results show that in the doping case, antiferromagnetism is suppressed by $J_\perp$ interaction, and the superconductivity is enhanced. At half filling, the superconductivity does not emerge even if the antiferromagnetism is suppressed by increasing the interaction strength. The antiferromagnetism does not increase or decrease monotonically with interaction strength U, and it has a peak around $U = 1.25$. The optimal doping of SC is dependent on $J_\perp/J_z$ and becomes slightly larger when J_z dominates. The finite-size scaling results are qualitatively consistent with the correlation lengths. Our results may contribute some aspects to the understanding of superconductivity and its parent materials and may also stimulate further cold-atom experiments to realize such a model to tune the competition between SC and AFM order in one system.
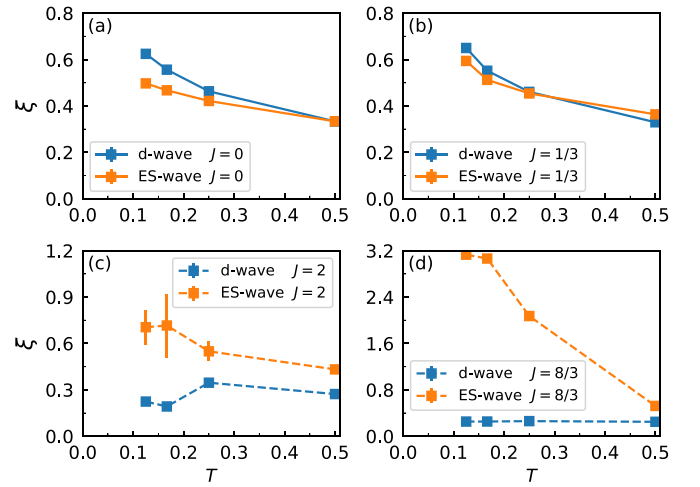
ACKNOWLEDGMENTS

FIG. 9. (a)–(d) Correlation lengths of extended s-wave (ES-wave) and d-wave superconducting pairings at $L = 8$, $U = 2.0$, and doping $x = \frac{1}{6}$. Here, $J_z = J_\perp = J$, and T is temperature.

APPENDIX

To demonstrate the impact of J on superconducting pairing symmetries, here we show some results of different J at $U = 2.0$. Since the relation $4U = J_z + 2J_\perp$ is broken, the sign problem will be serious, so we resort to a finite-temperature algorithm, the determinant quantum Monte Carlo (DQMC) method [42]. For the single-layer Hubbard model, d-wave pairing symmetry is the dominant pairing symmetry. Here we investigate the d-wave pairing defined in the first layer, and the order parameter can be written as

$$\Delta_i^d = c_{i1\uparrow}c_{i+\mathbf{x}1\downarrow} - c_{i1\downarrow}c_{i+\mathbf{x}1\uparrow} - c_{i1\uparrow}c_{i+\mathbf{y}1\downarrow} + c_{i1\downarrow}c_{i+\mathbf{y}1\uparrow}.$$
(A1)

Using Eqs. (5) and (6), we can get the correlation length of d-wave pairing. We also calculate the extended s-wave pairing defined in the main text. The results are shown in Fig. 9.

One can see that in Fig. 9, the d-wave pairing is dominant at small J, and the extended s-wave pairing is dominant at large J. In addition, the extended s-wave pairing saturates early compared with d-wave pairing; as one can see in Fig. 9(b), the d-wave pairing exceeds extended s-wave pairing at low temperature, and it grows faster than extended s-wave pairing at small J. Even though the sign problem stops us from performing simulations at lower temperature, a transition from d-wave pairing to extended s-wave pairing is also revealed as J increases in our simulations.

[1] E. Dagotto, Correlated electrons in high-temperature superconductors, Rev. Mod. Phys. **66**, 763 (1994).

[2] J. G. Bednorz and K. A. Müller, Possible high T_c superconductivity in the Ba-La-Cu-O system, Z. Phys. B **64**, 189 (1986).

[3] D. J. Scalapino, A common thread: The pairing interaction for unconventional superconductors, Rev. Mod. Phys. **84**, 1383 (2012).

[4] P. Dai, Antiferromagnetic order and spin dynamics in iron-based superconductors, Rev. Mod. Phys. **87**, 855 (2015).

[5] J. A. Sobota, Y. He, and Z.-X. Shen, Angle-resolved photoemission studies of quantum materials, Rev. Mod. Phys. **93**, 025006 (2021).

[6] C. N. Varney, C.-R. Lee, Z. J. Bai, S. Chiesa, M. Jarrell, and R. T. Scalettar, Quantum Monte Carlo study of the

two-dimensional fermion Hubbard model, Phys. Rev. B **80**, 075116 (2009).

[7] J. E. Hirsch and S. Tang, Antiferromagnetism in the Two-Dimensional Hubbard Model, Phys. Rev. Lett. **62**, 591 (1989).

[8] F. Šimkovic, J. P. F. LeBlanc, A. J. Kim, Y. Deng, N. V. Prokof'ev, B. V. Svistunov, and E. Kozik, Extended Crossover from a Fermi Liquid to a Quasiantiferromagnet in the Half-Filled 2D Hubbard Model, Phys. Rev. Lett. **124**, 017003 (2020).

[9] C. M. Varma, P. B. Littlewood, S. Schmitt-Rink, E. Abrahams, and A. E. Ruckenstein, Phenomenology of the Normal State of Cu-O High-Temperature Superconductors, Phys. Rev. Lett. **63**, 1996 (1989).

[10] J. M. Tranquada, B. J. Sternlieb, J. D. Axe, Y. Nakamura, and S. Uchida, Evidence for stripe correlations of spins and holes in copper oxide superconductors, Nature (London) **375**, 561 (1995).

[11] T. A. Maier and D. J. Scalapino, Pair structure and the pairing interaction in a bilayer Hubbard model for unconventional superconductivity, Phys. Rev. B **84**, 180513(R) (2011).

[12] U. Schollwöck, The density-matrix renormalization group, Rev. Mod. Phys. **77**, 259 (2005).

[13] P. H. Acioli, Review of quantum Monte Carlo methods and their applications, J. Mol. Struct.: THEOCHEM **394**, 75 (1997).

[14] G. Kotliar, S. Y. Savrasov, K. Haule, V. S. Oudovenko, O. Parcollet, and C. A. Marianetti, Electronic structure calculations with dynamical mean-field theory, Rev. Mod. Phys. **78**, 865 (2006).

[15] T. Aimi and M. Imada, Does simple two-dimensional Hubbard model account for high-T_c superconductivity in copper oxides? J. Phys. Soc. Jpn. **76**, 113708 (2007).

[16] C. Wen, X. Zhu, N. Hao, H. Guo, and S. Feng, Unconventional ferromagnetism and spin-triplet superconductivity in the imbalanced kagome-lattice Hubbard model, Phys. Rev. B **105**, 245131 (2022).

[17] B. Nosarzewski, E. W. Huang, P. M. Dee, I. Esterlis, B. Moritz, S. A. Kivelson, S. Johnston, and T. P. Devereaux, Superconductivity, charge density waves, and bipolarons in the Holstein model, Phys. Rev. B **103**, 235156 (2021).

[18] P. Mai, G. Balduzzi, S. Johnston, and T. A. Maier, Pairing correlations in the cuprates: A numerical study of the three-band Hubbard model, Phys. Rev. B **103**, 144514 (2021).

[19] Y.-X. Zhang, H.-M. Guo, and R. T. Scalettar, Charge density wave order on a π-flux square lattice, Phys. Rev. B **101**, 205139 (2020).

[20] T. Ma, L. Zhang, C.-C. Chang, H.-H. Hung, and R. T. Scalettar, Localization of Interacting Dirac Fermions, Phys. Rev. Lett. **120**, 116601 (2018).

[21] T. Hodson, J. Willsher, and J. Knolle, One-dimensional long-range Falikov-Kimball model: Thermal phase transition and disorder-free localization, Phys. Rev. B **104**, 045116 (2021).

[22] G. Fleury and X. Waintal, Numerical Finite Size Scaling Approach to Many-Body Localization, Phys. Rev. Lett. **100**, 076602 (2008).

[23] G. Pan, X. Zhang, H. Li, K. Sun, and Z. Y. Meng, Dynamical properties of collective excitations in twisted bilayer graphene, Phys. Rev. B **105**, L121110 (2022).

[24] V. Peri, Z.-D. Song, B. A. Bernevig, and S. D. Huber, Fragile Topology and Flat-Band Superconductivity in the Strong-Coupling Regime, Phys. Rev. Lett. **126**, 027002 (2021).

[25] X. Y. Xu, K. T. Law, and P. A. Lee, Kekulé valence bond order in an extended Hubbard model on the honeycomb lattice with possible applications to twisted bilayer graphene, Phys. Rev. B **98**, 121406(R) (2018).

[26] T. Huang, L. Zhang, and T. Ma, Antiferromagnetically ordered Mott insulator and d + id superconductivity in twisted bilayer graphene: a quantum Monte Carlo study, Sci. Bull. **64**, 310 (2019).

[27] B.-X. Zheng, C.-M. Chung, P. Corboz, G. Ehlers, M.-P. Qin, R. M. Noack, H. Shi, S. R. White, S. Zhang, and G. K.-L. Chan, Stripe order in the underdoped region of the two-dimensional Hubbard model, Science **358**, 1155 (2017).

[28] M. Qin, C.-M. Chung, H. Shi, E. Vitali, C. Hubig, U. Schollwöck, S. R. White, and S. Zhang (Simons Collaboration on the Many-Electron Problem), Absence of Superconductivity in the Pure Two-Dimensional Hubbard Model, Phys. Rev. X **10**, 031016 (2020).

[29] Z.-X. Li, Y.-F. Jiang, and H. Yao, Solving the fermion sign problem in quantum Monte Carlo simulations by Majorana representation, Phys. Rev. B **91**, 241117(R) (2015).

[30] M.-S. Vaezi, A.-R. Negari, A. Moharramipour, and A. Vaezi, Amelioration for the Sign Problem: An Adiabatic Quantum Monte Carlo Algorithm, Phys. Rev. Lett. **127**, 217003 (2021).

[31] S. Zhang, J. Carlson, and J. E. Gubernatis, Constrained path Monte Carlo method for fermion ground states, Phys. Rev. B **55**, 7464 (1997).

[32] R. Mondaini, S. Tarat, and R. T. Scalettar, Quantum critical points and the sign problem, Science **375**, 418 (2022).

[33] T. Ma, D. Wang, and C. Wu, Doping-driven antiferromagnetic insulator-superconductor transition: A quantum Monte Carlo study, Phys. Rev. B **106**, 054510 (2022).

[34] P. T. Dumitrescu, M. Serbyn, R. T. Scalettar, and A. Vishwanath, Superconductivity and nematic fluctuations in a model of doped FeSe monolayers: Determinant quantum Monte Carlo study, Phys. Rev. B **94**, 155127 (2016).

[35] A. Bohrdt, L. Homeier, I. Bloch, E. Demler, and F. Grusdt, Strong pairing in mixed-dimensional bilayer antiferromagnetic Mott insulators, Nat. Phys. **18**, 651 (2022).

[36] P. A. Lee, N. Nagaosa, and X.-G. Wen, Doping a Mott insulator: Physics of high-temperature superconductivity, Rev. Mod. Phys. **78**, 17 (2006).

[37] C. Wu and S.-C. Zhang, Sufficient condition for absence of the sign problem in the fermionic quantum Monte Carlo algorithm, Phys. Rev. B **71**, 155115 (2005).

[38] C. Wu, J.-P. Hu, and S.-C. Zhang, Exact SO(5) Symmetry in the Spin-3/2 Fermionic System, Phys. Rev. Lett. **91**, 186402 (2003).

[39] F. Parisen Toldin, M. Hohenadler, F. F. Assaad, and I. F. Herbut, Fermionic quantum criticality in honeycomb and π-flux Hubbard models: Finite-size scaling of renormalization-group-invariant observables from quantum Monte Carlo, Phys. Rev. B **91**, 165108 (2015).

[40] M. Campostrini, A. Pelissetto, and E. Vicari, Finite-size scaling at quantum transitions, Phys. Rev. B **89**, 094516 (2014).

[41] F. F. Assaad and I. F. Herbut, Pinning the Order: The Nature of Quantum Criticality in the Hubbard Model on Honeycomb Lattice, Phys. Rev. X **3**, 031010 (2013).

[42] J. E. Hirsch, Two-dimensional Hubbard model: Numerical simulation study, Phys. Rev. B **31**, 4403 (1985).